Usage guidelines

A Novel Adaptive Spectrum Noise Cancellation Approach for Enhancing Heartbeat Rate Monitoring in a Wearable Device

DONG YANG[1], YONGQIANG CHENG [ID][2], JIN ZHU[1], DONGFEI XUE [ID][2], GRANT ABT[3], HANGYANG YE[1], AND YONGHONG PENG[4]

[1]Department of Control Science and Engineering, Tongji University, Shanghai 201804, China
[2]School of Engineering and Computer Science, University of Hull, Hull HU6 7RX, U.K.
[3]School of Life Sciences, University of Hull, Hull HU6 7RX, U.K.
[4]Faculty of Computer Science, University of Sunderland, Sunderland SR6 0DD, U.K.

Corresponding author: Yongqiang Cheng (y.cheng@hull.ac.uk)

ABSTRACT This paper presents a novel approach, adaptive spectrum noise cancellation (ASNC), for motion artifacts removal in photoplethysmography (PPG) signals measured by an optical biosensor to obtain clean PPG waveforms for heartbeat rate calculation. One challenge faced by this optical sensing method is the inevitable noise induced by movement when the user is in motion, especially when the motion frequency is very close to the target heartbeat rate. The proposed ASNC utilizes the onboard accelerometer and gyroscope sensors to detect and remove the artifacts adaptively, thus obtaining accurate heartbeat rate measurement while in motion. The ASNC algorithm makes use of a commonly accepted spectrum analysis approaches in medical digital signal processing, discrete cosine transform, to carry out frequency domain analysis. Results obtained by the proposed ASNC have been compared with the classic algorithms, the adaptive threshold peak detection and adaptive noise cancellation. The mean (standard deviation) absolute error and mean relative error of heartbeat rate calculated by ASNC is 0.33 (0.57) beats $\cdot$ min^{-1} and 0.65%, by adaptive threshold peak detection algorithm is 2.29 (2.21) beats $\cdot$ min^{-1} and 8.38%, by adaptive noise cancellation algorithm is 1.70 (1.50) beats $\cdot$ min^{-1} and 2.02%. While all algorithms performed well with both simulated PPG data and clean PPG data collected from our verity device in situations free of motion artifacts, ASNC provided better accuracy when motion artifacts increase, especially when motion frequency is very close to the heartbeat rate.

INDEX TERMS Adaptive spectrum noise cancellation, heartbeat rate measurement, wearable device, PPG, motion artifacts.

I. INTRODUCTION

In aging societies, stroke and cardiovascular diseases [1] have become the main causes of disability and death [2]. Recent figures shows mortality caused by diseases of the heart among older people ($\geq$60 years) constitute up to 70% of deaths in the United States [3]. In addition, the aging population creates unprecedented challenges for long-term care in many countries around the world [4]. Heartbeat Rate (HR) is one of the physiological parameters commonly used in medical monitoring systems in older people, hence the continuous monitoring of heart activities has been deemed as a key enabler in tackling this challenge.

With advances in the development of microprocessors and micro-sensors, many conventional medical measurements can now be obtained using sophisticated clinical instruments. The data from these measurements can be processed in real-time using high-speed chips, with the data being transmitted to mobile phones or personal computers through low-power wireless communication technology [5]. Wearable medical devices do not only provide low-load and non-invasive health measurement, but also a long term and convenient way to continuously monitor elderly people without disturbing their life or impacting their normal lifestyle [6].

One of the methods used for non-invasive health measurement is Photoplethysmography (PPG). This method is considered to be the most effective and practical means in wearable devices [7] for monitoring the cardiovascular activities. PPG signal is often obtained using a biosensor

that illuminates the skin via a light source and detects the emission density reflected back or through body from that light source. This method can detect blood volume changes in the microvascular tissue based on the change in blood color as the pulse wave travels through the tissue [8]. Cui *et al.* [9] showed experimental results that the peak wavelength sensitivity to blood pulsations ranges from 510 nm to 590 nm, so green light with a wavelength of 525 nm is usually chosen for the PPG light source in integrated biosensors.

The capability to detect subtle changes in heart activities requires accurate HR measurement. Due to the indirect measurement nature, wearable devices inevitably face challenges caused by baseline drift and Motion Artifacts (MAs), especially during exercise and under free living conditions [10]. Although the classical Adaptive Threshold Peak Detection (ATPD) algorithm is capable of resolving baseline drift in PPG signal analysis by detection of peak positions in the time domain [11], ATPD is extremely vulnerable to MAs. Adaptive Noise Cancellation (ANC) has the ability to reduced unwanted MAs by introducing multi-sensor accelerometer and gyroscope signals and it is being widely used for cancelling MAs and noise in PPG signals [12]. However, the ANC algorithm fails if the MAs have a close enough main frequency component to the heartbeat rate in the PPG signal. Spectrum Subtraction (SS) has been another stream of widely adopted noise cancellation method in PPG signals analysis [13]–[15]. Fukushima *et al.* [14] subtracted the spectrum of acceleration data from the measured PPG signal to get the clean heartbeat signal. Y. Zhang *et al.* [15] combined the Ensemble Empirical Mode Decomposition (EEMD) with SS method to remove undesirable MAs in a wrist-type device and track HR changes during subjects' physical activities. Subtraction of spectrum works if the amplitude and envelope of frequency spectrum can be predefined but it is not suitable for situations where signal amplitude and envelope changes dynamically.

In this paper, adaptive spectrum noise cancellation approach is proposed to obtain accurate HR measurement in free living condition or during physical exercise. ASNC adaptively incorporates the motion artifacts spectrum data obtained from a multi-sensor accelerometer and gyroscope to remove motion noise contained in PPG signals in frequency domain. Simulation and experimental results have shown that ASNC performs more robustly than spectrum subtraction method and outperforms the ATPD and ANC algorithms quantitatively based on the measured HR in mean±standard deviation matrix.

The rest of the paper is organized as following: Section II states the background of the PPG foundation and the related work about ATPD and ANC algorithms. Section III introduces the ASNC algorithm theory and structure. Section IV describes the simulation, experiment and comparison of the algorithm. Section V concludes the paper with future work.

II. BACKGROUND
A. PPG FOUNDATION
Since PPG was first proposed by Hertzman, it has gained widespread use in recent years [16]. The PPG signal carries information about the cardiovascular system such as HR, oxygen saturation (SpO2), respiration and blood pressure [17]. It is often applied to take measurement at the skin surface, such as the fingertip, earlobe, forehead and wrist in non-invasive, low-cost and portable biosensors [18].
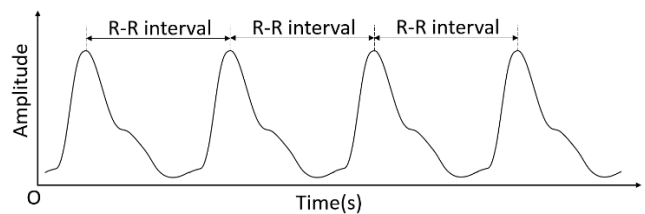

FIGURE 1. PPG signal with heartbeat rate R-R time interval.

A typical PPG pulse signal measured by reflective sensor is shown in FIGURE 1. The HR, which is the frequency of heart contractions measured as the number of beats per minute (beats $\cdot$ min^{-1}), is the basic vital sign extracted from PPG and related to the safety and death of human beings [19]. HR is normally calculated by using the R-R interval.

The normal resting HR of an adult human ranges from 60-100 beats $\cdot$ min^{-1} [3], which is defined in situations when a person is awake and calm. For elite athletes, it is common to have a resting HR between 36 and 50 beats $\cdot$ min^{-1}. The maximum HR (HR$_{max}$) is the highest HR that a person can achieve during progressive maximal exercise, and decreases with age [20] with an approximation formula $HR_{max} = 220 - Age$. It is often chosen 0.8 Hz – 3.0 Hz representing a HR range from 48-180 beats $\cdot$ min^{-1} as the pass band filter range.
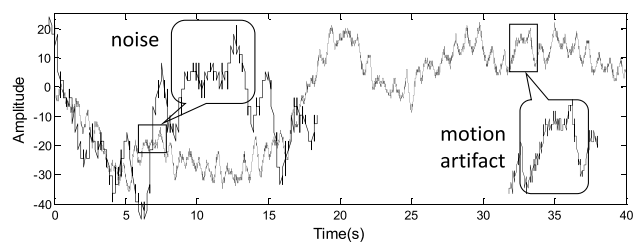

FIGURE 2. PPG raw signal measured on the wrist by a wearable watch in motion. The distortions include noise, motion artifact together with the baseline drift.

There are other factors affecting the measurement of clean PPG signals. Those challenges are the noise introduced by respiration, ambient light disturbance from sunlight, electricity frequency noise and motion artifacts [21]. FIGURE 2 is a sample of PPG raw signal obtained from a wrist wearable device, showing the distortions caused by noise and artifacts:

As shown in FIGURE 2, one can see that the baseline drift varies severely and the HR peaks are merged within

the MAs peaks. The baseline drift (a slowly varying signal in PPG) originated from a low frequency disturbance in the PPG signal caused by respiration and the autonomic nervous system [22]. To overcome the baseline drift, researchers have proposed many filtering approaches based on the frequency characteristics of PPG signals and noise [23], such as infinite impulse response (IIR) filter and finite impulse response (FIR) filter. The IIR bandpass filter is easy to design and performs well for detrending the baseline wander and minimizing undesirable distortion [24], thus often chosen to preprocess the PPG signal.

Researches have also been focused to overcome the MAs due to movement of wrist or body that distort the PPG raw signal [25]. Naraharisetti and Bawa [26] reviewed and compared five common signal processing methods for MAs cancellation, i.e. the ANC, Independent Component Analysis (ICA), Singular Value Decomposition (SVD), Wavelet Transform (WT) and cycle by cycle Fourier Series Analysis (FSA). It was shown that ANC has good tolerance to relatively small distortions from MAs. Santos *et al.* [24] presented a solution using accelerometer data to remove MAs on a LAVIMO device for physical exercise utilizing ANC and achieved a satisfactory result. Although ANC is a valuable algorithm for MAs reduction, clean PPG signal and MAs share a superimposed frequency zone which makes it difficult for the general IIR filter, ATPD or ANC to suppress MAs.

B. ADAPTIVE THRESHOLD PEAK DETECTION

The ATPD algorithm has played important role for temporal signal analysis that depends on peak positions [11], [27]. In mathematics, a peak is a local maximum point [27] that can be identified by detections of zero-crossings in the differences (slope sign change) between a point and its neighbors in the time domain. The use of ATPD algorithm on PPG signal was reported by H. S. Shin *et al.* in his work [28].

The ATPD algorithm deals with local maxima or minima detection in waveforms. When the algorithm is used to detect the peaks in PPG signal to calculate HR, an adaptive threshold needs to be applied to differentiate good (valid) or bad (invalid) peaks that should contribute to count the number of actual heartbeats. With the number of valid heartbeat peaks in a given duration of time, HR can be calculated by (1):

$$HR = 60 \times N_{peaks}/\Delta t \tag{1}$$

where N_{peaks} is the number of valid peaks, and Δt is the time interval in seconds between the first peak and the last peak.

As shown in the FIGURE 3, ATPD algorithm performs well in situations with baseline drift by elimination of the smaller peaks based on the amplitude and time interval from the local maxima. However, when the PPG signal is mixed with strong MAs resulting in significant baseline increment or decrement, the adaptive threshold method will fail in correctly picking up the peaks, e.g. the peaks at about 11 and 13 s are missed due to significant baseline decrement.
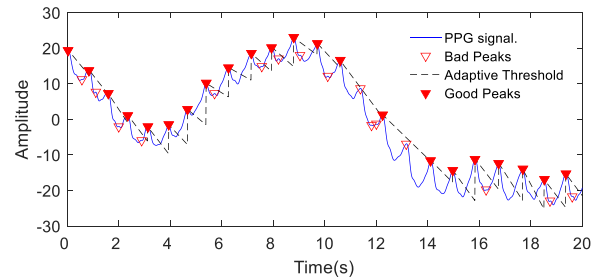

FIGURE 3. The result by adaptive threshold peak detection for filtered PPG signals in HR measurement.

C. ADAPTIVE NOISE CANCELLATION

ANC is a time domain approach to estimate clean signal distorted by additive noise or interference [29]. The ANC algorithm is widely used to remove noise in biological signals, especially PPG. The basic idea of the ANC algorithm is to suppress the noise and MAs in the distorted PPG signal through an adaptive filter. The method uses a primary input containing the expected signal and a reference input containing noise highly correlated with the primary signal in some unknown way [30]. The raw PPG signals measured by optical biosensor is a mixture of primary and reference input containing heartbeat and MAs; The data obtained by accelerometer and/or gyroscope [24] can be used as reference input to estimate MAs. As a result, MAs as the reference signal are adaptively subtracted from the raw PPG signal to reveal the primary input, i.e. the clean PPG signal.
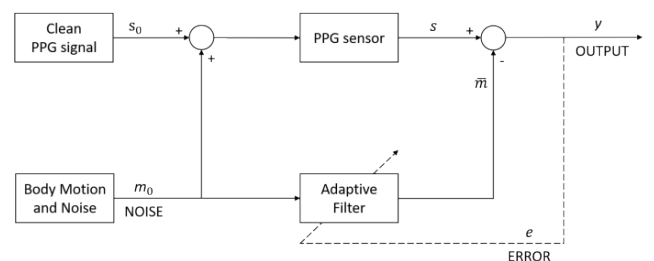

FIGURE 4. The block diagram of the ANC algorithm. s_0 is the clean PPG signal and primary input of the system, s is the raw PPG signal measured by a PPG sensor, m_0 is the MAs and reference input of the system, $\bar{m}$ is the estimation of the MAs calculated by the adaptive filter. The output of ANC is y which is the estimated data that best fit to clean PPG signal.

As shown in FIGURE 4, the raw PPG signal is calculated by the following equation:

$$s = \alpha(s_0 + m_0) \tag{2}$$

where α is the gain factor between the PPG signal and biosensor output. For simplicity without losing generality, the multiplication factor α is assumed to be equal to 1 in the digital signal processing computation.

Given $= s - \bar{m}$, $\alpha = 1$ and taking expectations of both sides of (2), one has:

$$E(y^2) = E[(s_0 + m_0 - \bar{m})^2]$$
$$= E(s_0^2) + 2E[s_0(m_0 - \bar{m})] + E[(m_0 - \bar{m})^2] \tag{3}$$

The signal energy $E\left(s_0^2\right)$ represents the mean of the squared amplitude [31]. The raw PPG signal s_0 is independent from the MAs disturbance m_0 and estimation $\bar{m}$ resulting in $2E[s_0(m_0 - \bar{m})]$ approaches to 0. In the meantime, s_0 has no input to the adaptive filter, thus the adjustment of the adaptive filter to minimize $E\left(y^2\right)$ will not affect the signal energy $E\left(s_0^2\right)$. Hence, the minimum output energy for (3) is:

$$min\, E\left(y^2\right) = E\left(s_0^2\right) + min\, E[(m_0 - \bar{m})^2] \qquad (4)$$

Minimizing $E\left(y^2\right)$ corresponds to minimizing $E[(m_0 - \bar{m})^2]$ and MAs estimation will approach to m_0. In other words, y is the least-squares estimation of s_0.

Based on the above correlation analysis, a dynamic adaptive model predicting the distortion of the PPG signal in response to acceleration and rotation can be built. The adaptive filter model can be implemented as a Least Mean Square (LMS) filter and Recursive Least Square (RLS) filter. In practice, the adaptive filter is often based on a FIR-type LMS filter with a specific time window. The coefficients of the adaptive filter are then calculated in real-time to minimize the output energy thus obtaining the MAs estimation.

III. ADAPTIVE SPECTRUM NOISE CANCELLATION
A. OVERALL STRUCTURE
In this section, the ASNC approach for suppression of MAs from distorted PPG signals in the frequency domain is presented to improve the accuracy of HR measurement. The proposed ASNC algorithm is composed of three steps: (1) Raw data collection and processing; (2) time domain to frequency domain conversion and (3) adaptive MAs removal and HR calculation. The flowchart is shown in Fig. 5.

Step 1: Raw data collection and preprocessing. The onboard biosensor samples the raw PPG and the integrated accelerometer and gyroscope tracks the motion acceleration and angular velocity data. Both data sets are sent to mobile devices over low energy Bluetooth ready for further analysis. On mobile devices, PPG raw data is preprocessed by a bandpass IIR filter to eliminate the low frequency baseline shift and most of the high frequency noise whist the motion data is pre filtered by a low-pass IIR filter. The filtered motion data is referred as the MAs Estimation (MAE) in the paper.

Step 2: Time domain to frequency domain conversion. All the pre-processed data are firstly segmented by sliding windows whose size is chosen to be approximately twice that of the maximum HR for adequate frequency resolution. Then the segmented data are fed into Discrete Cosine Transform (DCT) process to be converted into frequency domain. Finally, the envelope detection smooths out the outline of the signal envelop by cubic spline to compute the contours of PPG and MAs spectrum in the frequency domain.

Step 3: Adaptive MAs removal and HR calculation. In this step, the MAs spectral contour is adapted to an equivalent amplitude and phase to the one contained in the PPG signal so that by subtracting the MAs contour envelop from the PPG spectral envelope in the frequency domain the clean PPG
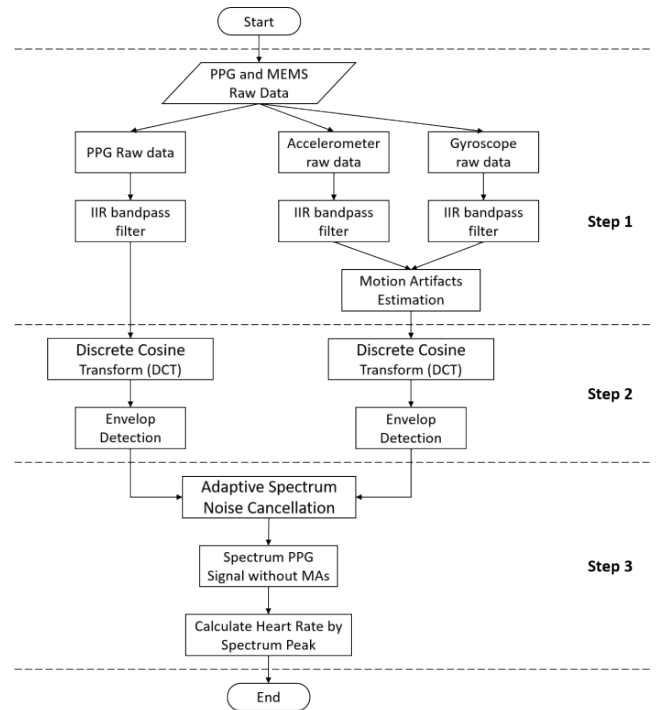

FIGURE 5. Flowchart of the Adaptive Spectrum Noise Cancellation (ASNC) algorithm.

can be revealed. Finally, a main-harmonic frequency peak decision tree is used to pick up the appropriate peak in the clean PPG within the HR frequency zone to calculate the HR.

B. ADAPTATION PROCESS
Assumption[1]*:* The clean PPG signal is independent from MAs disturbance and MAs disturbance is digitally overlapped with the clean PPG signal through a linear physical process [32]. The noises introduced by respiration, environmental light and electricity fluctuations can be filtered by appropriately designed IIR band filter.

FIGURE 6 shows the proposed ASNC algorithm block diagram.

The objective of the ASNC algorithm is to find an optimal system output y that can best fit to the clean PPG signal s_0. The raw PPG data s compromises of the clean PPG signal s_0, MAD w and noise u:

$$s = \alpha(s_0 + w + u) \qquad (5)$$

where u is the noise from environmental light disturbance and baseline shift.

According to our Assumption, the MAE m read by accelerometer and gyroscope can be linearly represented by

---

[1]Although moving bodies will affect one's HR and cause the change of clean PPG signal, this variance can be compensated by the rapid updated measurements. There is a mechanism to avoid PPG signal saturation, hence the measurement of PPG signal can be treated as a linear process. Wrist motion can be measured by accelerometers and gyroscopes which are related to MAs in linear fashion [40]. There are other kinds of noise as the secondary disturbance in the algorithm.
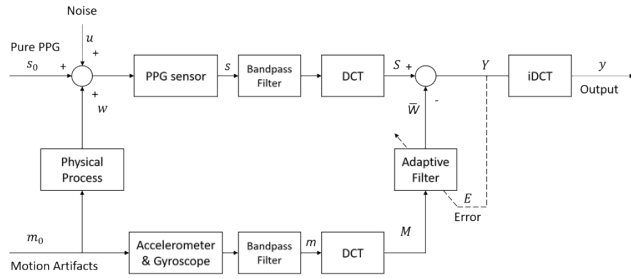
FIGURE 6. Adaptive spectrum noise cancellation algorithm block diagram. The lowercase letters represent the continuous-time domain signal and the capital letters represent the corresponding signal in the frequency domain.

motion artifact m_0 as below:

$$m = \beta m_0 \qquad (6)$$

where β is a constant coefficient.

The MAD w is the motion interference contained in the PPG biosensor readings through a physical process. w can be linearly represented as following:

$$w = \gamma m_0 \qquad (7)$$

where γ is a constant weight factor.

The time to frequency domain transformation is performed by the commonly used approach Fourier transform [33] shown below:

$$X \stackrel{\text{def}}{=} X(\xi) = \mathcal{F}[x(t)] = \int_{-\infty}^{\infty} x(t) e^{-2\pi i t\xi} dt \qquad (8)$$

where $x(t)$ is the time domain signal; i is the imaginary unit; the independent variable t represents time (in seconds), the transform variable ξ represents frequency (in hertz). The functions $x(t)$ and $X(\xi)$ are often referred as a Fourier transform pair.

Taking the Fourier transform on (5) gives:

$$S = \alpha(S_0 + W + U) \qquad (9)$$

where S, S_0, W, U represent the corresponding signal in spectrum s, s_0, w, u respectively.

Substitute (9) with $Y = S - \bar{W}$ and given the noise U being eliminated by band pass filter, one obtains:

$$Y = \alpha(S_0 + W) - \bar{W} \qquad (10)$$

Square both sides of (10):

$$Y^2 = \left[\alpha(S_0 + W) - \bar{W}\right]^2$$
$$= (\alpha S_0)^2 + 2\alpha S_0 (\alpha W - \bar{W}) + (\alpha W - \bar{W})^2 \qquad (11)$$

Taking expectations of both sides gives (12). As S_0 is the clean PPG signal spectrogram that is uncorrelated with the MAs spectrogram, expectation of $2\alpha S_0 (\alpha W - \bar{W})$ approaches to 0, hence it can be eliminated:

$$E[Y^2] = E[(\alpha S_0)^2] + E[(\alpha W - \bar{W})^2] + E[2\alpha S_0 (\alpha W - \bar{W})]$$
$$E[Y^2] \approx E[(\alpha S_0)^2] + E[(\alpha W - \bar{W})^2] \qquad (12)$$

Similar to (4), the objective of minimizing the error between MAE and MAD is equivalent to minimizing the output energy $E[Y^2]$:

$$min\, E[Y^2] \equiv E[(\alpha S_0)^2] + min\, E[(\alpha W - \bar{W})^2] \qquad (13)$$

When $E[Y^2]$ is minimized by the adaptive filter, the output $\bar{W}$ is then a best least squares estimation of αW. Furthermore, from (10), there is $Y - \alpha S_0 = \alpha W - \bar{W}$, that is when $E[(\alpha W - \bar{W})^2]$ is minimized, $E[(Y - \alpha S_0)^2]$ is also minimized.

Let $h(t)$ be the adaptive filter:

$$\bar{w} = h * m \qquad (14)$$

With the convolution theorem property of the FT: $X(\xi)Y(\xi) = \mathcal{F}[x(t) * y(t)]$, the Fourier transform form of (14) can be expressed as:

$$\bar{W} = HM = \beta H M_0 \qquad (15)$$

Similarly, (7) can be turned into $W = \gamma M_0$, thus:

$$\alpha W - \bar{W} = \alpha\gamma M_0 - \beta H M_0 = (\alpha\gamma - \beta H)M_0 \qquad (16)$$

When equation $E[(\alpha W - \bar{W})^2] = 0$ is satisfied, the output energy $E[Y^2] = E[(\alpha S_0)^2]$ reaches its minimum. The following key formulas can be concluded:

$$\alpha\gamma - H\beta = 0 \qquad (17)$$
$$H = \frac{\alpha\gamma}{\beta} \qquad (18)$$

Equation (18) indicates that H can be evaluated by constant variables, and the adaptive filter can lead to satisfy $\alpha W \approx \bar{W}$ and $Y \approx \alpha S_0$. As a result, the output will present the noise free clean signal.

C. MAS ESTIMATION

To evaluate the MAs signal which distorts the clean PPG signal, both the accelerometer and gyroscope are used in the device.

Micro tri-axial accelerometer is used to detect magnitude and direction of the three dimensional accelerations. It measures all forces that being applied on the sensor including the gravity vector. It works reliably over long time period. Every small force acting on the sensor will have effects on the measurements, hence the following formula is used to fuse the amplitudes of all acceleration components:

$$a = \sqrt{a_x^2 + a_y^2 + a_z^2} \qquad (19)$$

where a_x, a_y, a_z are the components of the three axes, a is the amplitude of acceleration.

A gyroscope is a spinning wheel or disc where the axis of rotation is free. The orientation of the spinning axis is unaffected by tilting when the wheel is spinning due to the conservation of angular momentum. Although the gyroscope can obtain accurate angular momentum that is not susceptible to external forces, the angular momentum calculated over

time by a gyroscope tends to drift. So, the gyroscope data is reliable only over the short term. The amplitude of gyroscope sensor readings is fused as following:

$$g = \sqrt{g_x^2 + g_y^2 + g_z^2} \qquad (20)$$

where g_x, g_y, g_z are the components of three axels, g is the amplitude of angular momentum.

By combing accelerometer and gyroscope, the MAs can be estimated as following:

$$m = \ell \cdot a + (1 - l) \cdot g \quad (0 \le l \le 1) \qquad (21)$$

where m is the estimation of MAs, i.e. MAD, ℓ is a weight factor to fuse accelerometer and gyroscope measurements.

D. ENVELOPE DETECTION
In digital signal processing, the transformed frequency spectrum from time data series by spectral analysis process using component frequencies identification is discrete and unsmooth. It is common practice to use envelope detector which connects all the peaks in the signal to smooth the contour of the discrete spectrum so that we can subtract two spectrums directly, e.g. the raw PPG and the noise contained in PPG signal.

There are two common methods of envelope detection, peak detection with interpolation [34] and Hilbert transform [35]. The first envelope detection method involves peaks detection by down sampled signal to reduce the sampling frequency, then intermediate values interpolation by a linear or spline method to smooth the signal. Then the signal is processed through a minimum-phase, lowpass filter to eliminate the high frequency energy to obtain the envelop.

The Hilbert transform envelope detection method involves creation of the analytic signal from the input using the Hilbert transform. An analytic signal is a complex signal, where the real part is the original signal and the imaginary part is the Hilbert transform of the original signal. Mathematically the envelope $e(t)$ of a signal $x(t)$ is defined as the magnitude of the analytic signal as shown in the following equation:

$$e(t) = \sqrt{x^2(t) + \hat{x}^2(t)} \qquad (22)$$

where $\hat{x}(t)$ is the Hilbert transform of $x(t)$. However, the envelope amplitude does not always match the actual signal and is computational power intensive. Hence, the peak detection with interpolation is selected in our system.

E. SPECTRUM ANALYSIS
The DFT is a common approach used to transform time series digital signals to the frequency domain [36]. DFT is defined as the following equation:

$$X_{DFT}(k) \overset{\text{def}}{=} \mathcal{F}[x(n)] = \sum_{n=0}^{N-1} x(n) e^{-2\pi i k n / N} \qquad (23)$$

where i is the imaginary unit; $x(0)$, $x(1)$, $x(2)$, ..., $x(N-1)$ are the N signal samples. These samples are further transformed into N periodic complex numbers:

$X_{DFT}(0)$, $X_{DFT}(2)$, ..., $X_{DFT}(N-1)$. The customary domain $k = 0, 1, ..., N-1$ is the frequency index.

In DFT, each $X(k)$ is a complex number that encodes both amplitude and phase. Since PPG and MAs signals are real valued data while DFT represent the transformed result in complex value form, half of the result in the frequency domain are redundant due to conjugate symmetry feature of the transformation.

The DCT converts a finite discrete sequence of data to a sum of real valued cosine function and is more suitable for handling the frequency domain data directly [37]. DCT also has ideal frequency filter characteristics [21] where frequencies are more concentrated on the major frequency components. Various forms of DCT definitions are designed for different applications. Below, the most commonly used DCT in signal processing is given:

$$X_{DCT}(k) = \sum_{n=0}^{N-1} x(n) \cos[\frac{\pi}{N}\left(n + \frac{1}{2}\right)k] \qquad (24)$$

where X_{DCT} is the DCT frequency domain data. The DFT is normally implemented by the Fast Fourier Transform (FFT) algorithm which has a complexity of $O(n\log n)$. DCT is a real number transform with better computational efficiency, whereas the Fast Discrete Cosine Transform (FDCT) algorithm takes only 1/6 as many steps as the FFT [38].
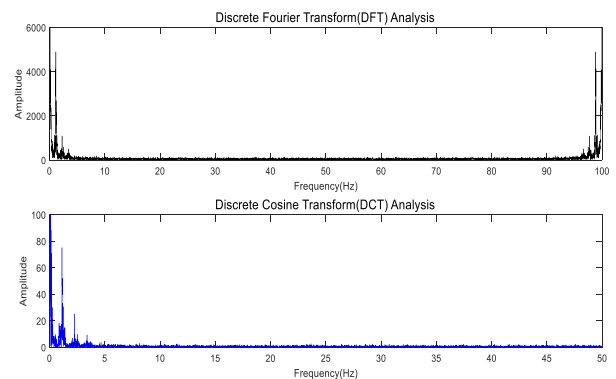

FIGURE 7. The comparison of DFT and DCT analysis. The spectrum of the DFT is symmetrical around the center frequency point, while the spectrum of the DCT only has a half of the frequency zone, i.e. the DCT is more efficient for spectrum analysis.

FIGURE 7 shows the comparison result of DFT and DCT frequency analysis.

Due to the dynamics of the MAs and individual differences in the PPG, the transformed amplitudes of PPG and MAs frequencies are often on different scales. The objective of the ASNC algorithm is to adjust the adaptive filter $h(t)$ to adaptively subtract the MAs signal from the distorted PPG signal.

Let $\hat{S}$ be PPG spectrum envelope, $\hat{M}$ be MAs spectrum envelope. What we need to find out is a suitable gain H that matches the spectrum amplitude of PPG and MAs in order to remove the $\hat{M}$ contained in $\hat{S}$. According to (13), this can be achieved by minimizing $E[Y^2]$, and we can calculate Y by the

smoothed spectrum envelope data as below:

$$min \, E[Y^2] \equiv min \, E(\hat{S} - \hat{M}H)^2 \qquad (25)$$

The objective is to minimize $(\hat{S} - \hat{M}H)^2$. Inverting the matrix of the normal equations, the algebraic solution of the normal equations can be written as:

$$H = \hat{M}^+ \hat{S} \qquad (26)$$

where $\hat{M}^+$ is the Moore–Penrose pseudoinverse of $\hat{M}$ and H is proper adaptive least mean squares filter.

The adaptive filter simulates the desired filter by searching the filter coefficients that minimize the least mean squared error signal (difference between the desired and the actual signal) in the frequency spectrum. It is a stochastic gradient descent method that the filter is only adapted based on the error.

IV. SIMULATION AND EXPERIMENT

In this section, we verify the efficacy of ASNC by applying it in both simulated and real life scenarios for HR measurement.

FIGURE 8. Verity wrist-wearable watch.

A. ADAPTIVE SPECTRUM NOISE CANCELLATION ON VERITY

The experimental platform is the Verity watch [1] shown in Fig. 8. Verity is a wrist-wearable device intended for continuous monitoring of users' HR. The optical biosensor on the back measures the PPG signal while the onboard tri-axial accelerometer and gyroscope sensors measure the MAs. The embedded 560 nm green light has been used for improved environmental noise tolerance compared to red light source. As the MAs introduced to the PPG have the same effects on the accelerometer and gyroscope sensors, the motions extracted can be used to compensate the MAs by using ASNC.

Data measured by Verity is transmitted to mobile devices using the Bluetooth low energy wireless protocol and segmented into chunks of 60s. The amplitude is normalized to 1.0. The sampling rate is 100 Hz for both PPG and MAs.

Fig. 9 shows a snapshot of both PPG signal and MAs taken by Verity when the hand is still. As seen in the figure, their amplitudes are in different order of scales, therefore the MAs contained in the PPG signal cannot be subtracted directly. However, the ANC algorithm will still try to amplify the noise signal to match the amplitude of the PPG signal causing an invalid extraction of the real PPG signal.
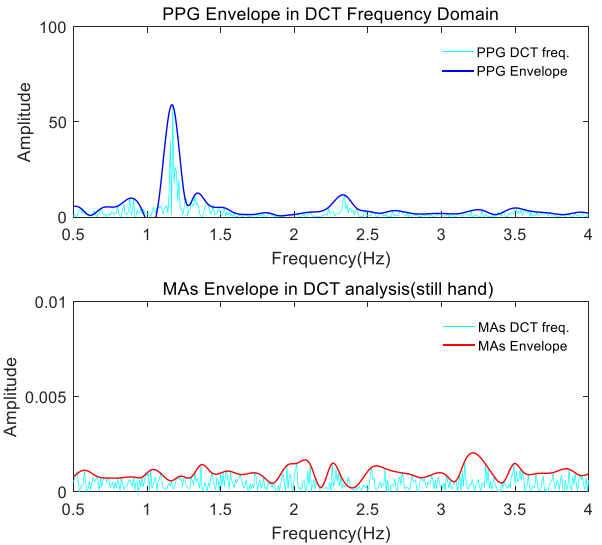

FIGURE 9. PPG and MAs signal envelope in DCT analysis, the PPG and MAs data are sampled at 100 Hz for 20s when the wrist is kept in still.
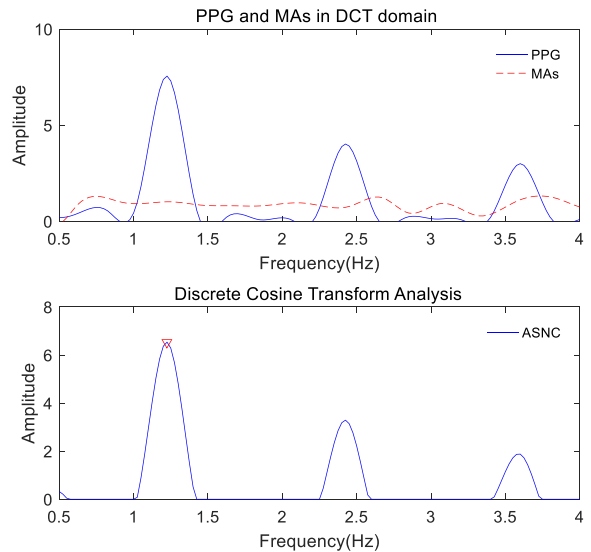

FIGURE 10. The result of ASNC with white noise artifacts.

By applying ASNC, the resultant spectrum are shown in FIGURE 10. The shape of MAs spectrum is adjusted by the adaptive algorithm to the same scale of noise in PPG, and can be eliminated properly via subtraction. The ASNC algorithm shows robust property based on the 'long tail' from 1.5 Hz to 4 Hz, and the HR frequency is the highest peak in the PPG spectrum.

This shows the robust performance of ASNC is irrelevant of the existence of noise compared to ANC.

To address the capability of ASNC dealing with challenges where MAs and HR have close enough frequency, FIGURE 11 data has been used. Both MAs and HR have frequency peaks around 1.3 Hz.

In Fig. 12, the MAs spectrum is adjusted through adaptive filtering and matched to its counterpart in the PPG spectrum.
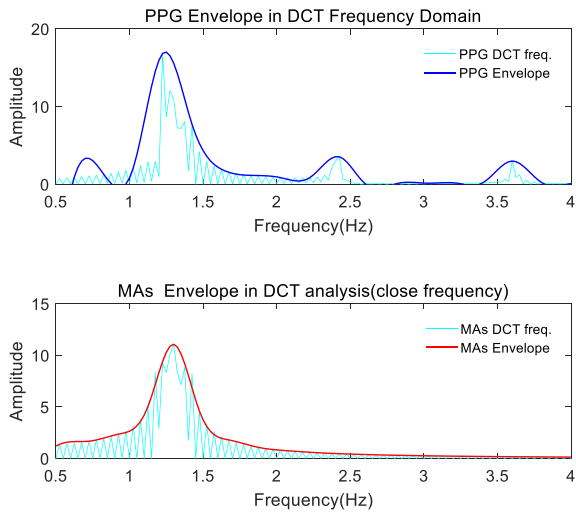
FIGURE 11. PPG and MAs signal envelope in DCT analysis. The peak frequency of PPG and motion artifacts are very close.
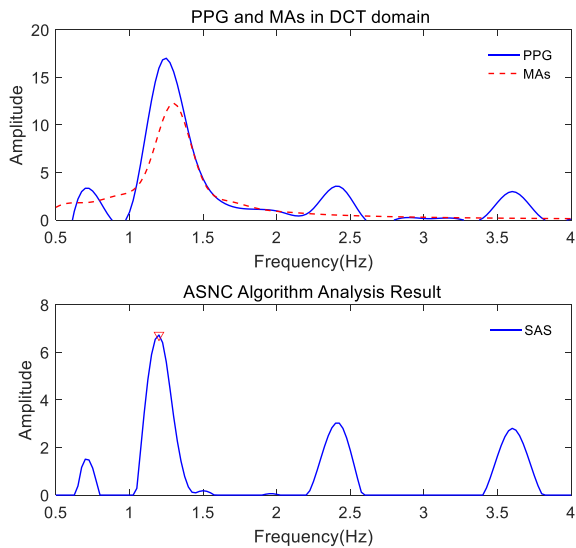

FIGURE 12. The result of ASNC with close frequency peak between PPG and motion artifacts.

FIGURE 13. Raw and bandpass filtered PPG signal measured by Verity.
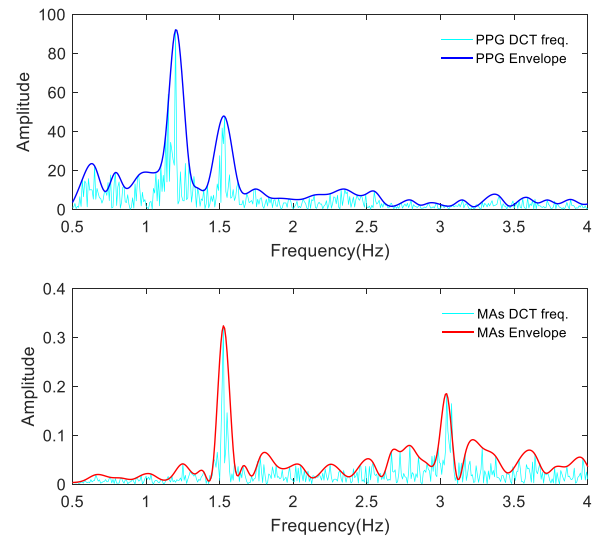
FIGURE 14. The envelope of PPG and MAs frequency spectrum.

Fig.12 shows the MAs has been removed from the raw PPG signal successfully and revealed the correct real PPG peaks.

As a real time HR measurement experiment. The HR was measured simultaneously by a CE marked medical device, called EIMO, designed and developed by iMonSys ltd. [39], [41].

Fig. 13 shows a frame of raw PPG signal sampled from Verity. Fig. 14 shows the PPG and MAs signal envelope in frequency domain. There are two peak frequencies in the PPG spectrum and both are within the range of human HR. The lower figure shows the details of MAs in the frequency domain, with a peak close to HR and some high frequency noise.

Fig. 15 shows the result after applying the adaptive filter. By the removal of MAs from the PPG signal, the second
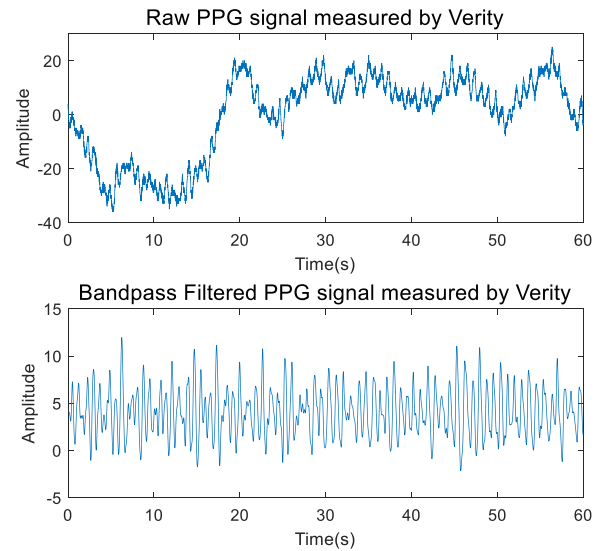
highest peak was eliminated and the HR can be correctly identified and calculated.

From Fig. 13, we can observe that the distortion is much more pronounced than the PPG signal without motion artifacts in the time domain. In Fig. 15, the motion peak is around 1.5 Hz and at the same time there are also 1.5 Hz peak in the PPG signal. Following application of the ASNC algorithm, the HR peak is revealed as 1.2 Hz. Measured by the EIMO device, the heart rate is 72 beats $\cdot$ min^{-1} which means 1.2 Hz is the frequency component for actual HR.

B. COMPARISON OF ATPD, ANC AND ASNC

To validate our proposed ASNC algorithm's performance against ATPD and ANC algorithms systematically, simulation models of PPG, MAs and baseline wander have been proposed for distorted PPG signal generation [21].
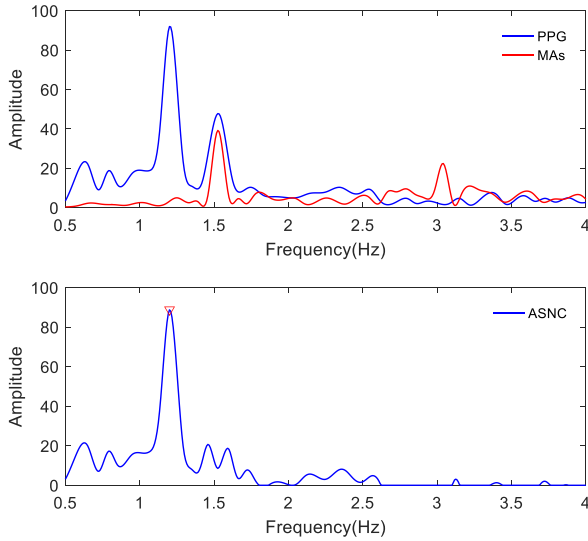
FIGURE 15. PPG raw data measured in wrist with motion artifact in time domain and displayed after discrete Fourier Transform in frequency domain.

By altering the parameters of the models, we can examine different combinations of HR and noises in a controlled manner.

1) SIGNAL MODELS

The major frequency component of a PPG signal is around 0.8-3.0 Hz. The low frequency wander component generally reflects the respiration (0.15–0.4 Hz) and baseline drift (0-0.1 Hz), and the MAs frequency is possible from 0 to signal sampling rates. The PPG signal is periodic and can be represented with the model below:

$$s_0 = A_0 f(t_0, f_0, HR_a) \tag{27}$$

where f is the model of the simulated clean PPG signal, A_b is the amplitude and assume it is 1.0, t_d is time duration set to 20 s, f_0 is sample frequency set to 100 Hz, HR_a is the actual HR.

The low frequency component of PPG contains the respiration effect which is measured when a person is at rest and involves counting the number of breaths for one minute. The respiration is removed by low-pass filter from the standard PPG signal, so we do not need to add extra signal to the PPG. Hence only baseline drift u_b is simulated and defined as below:

$$u_b = \sum_{f_s=0}^{0.1} A_b cos(2\pi f_b t + \varphi_b) \tag{28}$$

where A_b is the random amplitude of every frequency component from 0 to 1, f_b is the series of frequency points from 0 to 0.1 Hz which is the main baseline shift frequency component, t is the time series, φ_b is the random phase shift from 0 to π rad.

MAs are the dominant influential noise in PPG signals in the moving state. Therefore, the mathematical expression of MAs effect is designed by a frequency center-moving

digital signal, and cannot be easily removed by band pass filter. The MAs simulation model is defined as the following equation:

$$m_s = A_s cos(2\pi f_s t + \varphi_s) \tag{29}$$

where m_s is the noise of MAs simulation, f_s is the MAs frequency point which ranges from 0.5 Hz-10 Hz overlapping with the PPG signal. A_s is the random amplitude from 0 to 1.0 which is the same amplitude as the PPG signal. The phase delay φ_s is random from 0 to π rad.

The raw PPG signal is then the addition of all three signals:
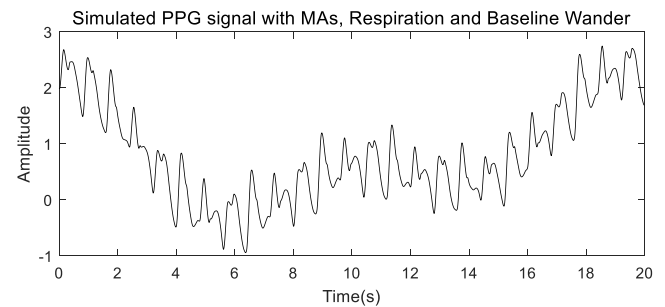
$$s = s_0 + m_s + u_b \tag{30}$$

FIGURE 16. Simulated PPG signal with baseline wander and MAs.

Fig. 16 shows a resultant PPG signal with a duration of 20 s sampled at 100 Hz. The HR randomly changes at every step. Variable s is the simulated signal which is the input of the three algorithms.

2) EVALUATION

Each simulated PPG signal is fed to all ATPD, ANC and ASNC algorithms for processing to obtain HR. Three criteria, the absolute error, relative error and standard deviation are used in our comparison. These criteria define a mathematical method for deriving the accuracy and uncertainty in the measurement, i.e. the difference between the calculated HR and the given HR used to generate the simulated PPG signal. The absolute error of HR shows the actual scale of measured error off the actual HR value, and the relative error shows how large the error is in relation to the true value.

The mean of the absolute error $E_{absolute}$ is defined as:

$$E_{absolute} = \frac{1}{N} \sum_{i=1}^{N} |HR_m(i) - HR_a(i)| \tag{31}$$

where the relative error is the ratio of the absolute error of the measured HR to the actual HR. The relative error expresses the 'relative size of the error' of the measurement in relation to the measurement itself.

The mean of the relative error $E_{relative}$ is calculated by the following equation:

$$E_{relative} = \frac{1}{N} \sum_{i=1}^{N} \frac{|HR_m(i) - HR_a(i)|}{HR_a(i)} \times 100\% \tag{32}$$
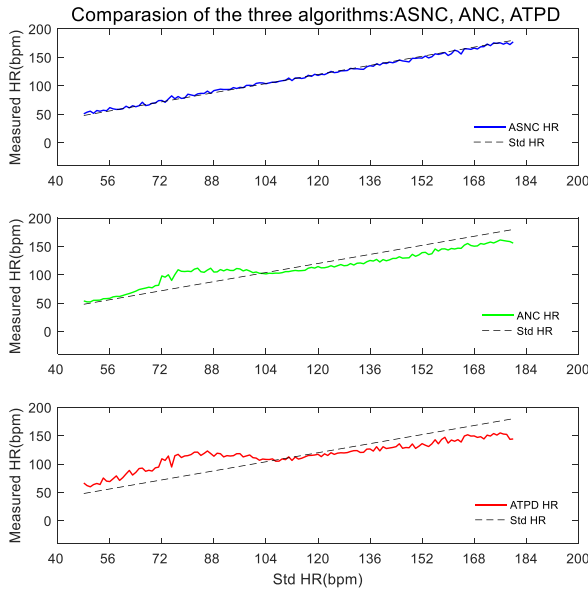
FIGURE 17. Comparison of the three algorithms in HR measurement against the simulated PPG signals with baseline shift and Mas. The HR ranges from 48 to 180 beats · min^{-1}.

The standard deviation (SD) denoted as σ is a measure to quantify the dispersion or variation of a set of data values around the mean:

$$\sigma = \sqrt{\frac{1}{N} \sum_{i=1}^{N} (HR_m(i) - HR_a(i))^2} \qquad (33)$$

In the experiment, the actual HR in the simulate PPG signal is simulated from 48 to 180 beats · min^{-1}, with each sample having a duration of 20 s. FIGURE 17 shows the results of the calculated HR_m by ATPD, ANC and ASNC algorithms with a mean of 10 attempts. One can see that the measured HR using the ASNC approach is much closer to the actual HR than the ATPD and ANC methods.

TABLE 1. The absolute error, relative error and standard deviation of the ATPD, ANC and ASNC algorithms with 10 different simulation datasets.

Case	ATPD			ANC			ASNC		
	E_a	E_r	σ	E_a	E_r	σ	E_a	E_r	σ
1	3.1	8.5%	2.1	1.2	2.3%	1.4	0.1	0.5%	0.5
2	1.8	8.0%	2.2	1.8	2.1%	1.6	0.2	0.4%	0.5
3	2.8	9.2%	2.3	1.6	2.3%	1.5	0.0	0.5%	0.6
4	3.1	9.8%	2.3	1.5	2.1%	1.4	0.3	0.3%	0.5
5	2.3	8.3%	2.2	2.0	1.7%	1.4	0.2	0.6%	0.6
6	0.7	6.5%	2.1	2.2	1.7%	1.5	0.0	0.8%	0.6
7	3.1	9.1%	2.3	1.5	2.3%	1.5	1.1	2.1%	0.7
8	1.6	7.5%	2.1	2.0	1.9%	1.5	0.3	0.9%	0.5
9	2.8	9.5%	2.3	1.3	2.7%	1.6	1.0	0.0%	0.7
10	1.6	7.4%	2.2	2.8	1.1%	1.6	0.0	0.4%	0.5

Table 1 shows the results of $E_{absolute}$ and the mean relative error $E_{relative}$. The mean (SD) absolute error $E_{absolute}$ of 0.32 (0.57) beats · min^{-1} for the proposed ASNC algorithm shows a significant improvement compared to ATPD and ANC methods.

TABLE 2. The mean Absolute Error, Relative Error and Standard Deviation of the ATPD, ANC and ASNC algorithm.

Mean/Method	ATPD	ANC	ASNC
$E_{absolute}$	2.29	1.79	0.32
$E_{relative}$	8.38%	2.02%	0.65%
σ	2.21	1.50	0.57

The following Table 2 shows the mean (SD) of the result:

All three algorithms work well without the presence of MAs, however the proposed new ASNC approach has shown a significant improvement for reducing baseline shift and MAs cancellation with more accurate HR measurements.

V. CONCLUSION

In this paper, the ASNC algorithm was proposed to remove MAs noise from raw PPG signals to obtain accurate HR when a human is in motion. The ASNC method consists of three key steps: obtain and preprocess raw PPG data; transform PPG and MAs signal from time domain to the frequency domain; adaptive spectrum subtraction to obtain the cleaned PPG spectrum profile for HR calculation.

We tested the ASNC algorithm on our wrist wearable platform Verity. This algorithm is able to remove MAs and calculate HR while in motion. In the ASNC algorithm, DCT shows more advantages than DFT in real number computing on magnitude response and phase distortion respects.

The ASNC algorithm has also been compared with ATPD and ANC using simulated PPG signals with motion. The ASNC achieves the lowest mean (SD) absolute error of 0.33 (0.57) beats · min^{-1} and mean relative error of 0.65%, compared to those obtained using ATPD (mean absolute error 2.29 (2.21) beats · min^{-1}; mean relative error 8.38%) and ANC (mean absolute error 1.70 (1.50) beats·min^{-1}; mean relative error 2.02%). The ASNC therefore shows a significant performance improvement compared with ATPD and ANC.

Despite the efficacy of DCT in the ASNC algorithm, compared with the time domain algorithm ATPD, the ASNC algorithm needs more memory and computational resource which currently hinders the adoption of the algorithm process on the Verity watch directly due to its limited hardware resources. The combination of ASNC with ATPD and ANC may be a direction for future research.

REFERENCES

[1] J. Winkley, P. Jiang, and W. Jiang, "Verity: An ambient assisted living platform," *IEEE Trans. Consum. Electron.*, vol. 58, no. 2, pp. 364–373, May 2012.

[2] S. C. Mukhopadhyay, "Wearable sensors for human activity monitoring: A review," *IEEE Sensors J.*, vol. 15, no. 3, pp. 1321–1330, Mar. 2015.

[3] D. Mozaffarian, "Heart disease and stroke statistics–2015 update: A report from the american heart association," *Circulation*, vol. 131, no. 4, pp. e29–e322, 2015.

[4] Z. Feng, C. Liu, X. Guan, and V. Mor, "China's rapidly aging population creates policy challenges in shaping a viable long-term care system," *Health Affairs*, vol. 31, no. 12, pp. 2764–2773, 2012.

[5] J. Allen, "Photoplethysmography and its application in clinical physiological measurement," *Physiol. Meas.*, vol. 28, no. 3, pp. R1–R39, 2007.

[6] Z. Zhang, Z. Pi, and B. Liu, "TROIKA: A general framework for heart rate monitoring using wrist-type photoplethysmographic signals during intensive physical exercise," *IEEE Trans. Biomed. Eng.*, vol. 62, no. 2, pp. 522–531, Feb. 2015.

[7] E. S. Winokur, T. O'Dwyer, and C. G. Sodini, "A low-power, dual-wavelength photoplethysmogram (PPG) SoC with static and time-varying interferer removal," *IEEE Trans. Biomed. Circuits Syst.*, vol. 9, no. 4, pp. 581–589, Aug. 2015.

[8] L. G. Lindberg, T. Tamura, and P. Å. Öberg, "Photoplethysmography," *Med. Biol. Eng. Comput.*, vol. 29, no. 1, pp. 40–47, Jan. 1991.

[9] W. Cui, L. E. Ostrander, and B. Y. Lee, "*In vivo* reflectance of blood and tissue as a function of light wavelength," *IEEE Trans. Biomed. Eng.*, vol. 37, no. 6, pp. 632–639, Jun. 1990.

[10] B. S. Kim and S. K. Yoo, "Motion artifact reduction in photoplethysmography using independent component analysis," *IEEE Trans. Biomed. Eng.*, vol. 53, no. 3, pp. 566–568, Mar. 2006.

[11] B.-L. Lee, B.-L. Lee, and W.-Y. Chung, "Smartwatch-based driver alertness monitoring with wearable motion and physiological sensor," in *Proc. 37th Annu. Int. Conf. IEEE Eng. Med. Biol. Soc.*, vol. 1. Aug. 2015, pp. 6126–6129.

[12] W. Harrison, J. Lim, and E. Singer, "A new application of adaptive noise cancellation," *IEEE Trans. Acoust., Speech, Signal Process.*, vol. ASSP-34, no. 1, pp. 21–27, Feb. 1986.

[13] T. Kleinschmidt, S. Sridharan, and M. Mason, "The use of phase in complex spectrum subtraction for robust speech recognition," *Comput. Speech Lang.*, vol. 25, no. 3, pp. 585–600, 2011.

[14] H. Fukushima, H. Kawanaka, M. S. Bhuiyan, and K. Oguri, "Estimating heart rate using wrist-type Photoplethysmography and acceleration sensor while running," in *Proc. Annu. Int. Conf. IEEE Eng. Med. Biol. Soc. (EMBS)*, Aug./Sep. 2012, pp. 2901–2904.

[15] Y. Zhang, B. Liu, and Z. Zhang, "Combining ensemble empirical mode decomposition with spectrum subtraction technique for heart rate monitoring using wrist-type photoplethysmography," *Biomed. Signal Process. Control*, vol. 21, pp. 119–125, Aug. 2015.

[16] A. B. Hertzman, "The blood supply of various skin areas as estimated by the photoelectric plethysmograph," *Amer. J. Physiol.-Legacy Content*, vol. 124, no. 2, pp. 328–340, 1938.

[17] R. W. C. G. R. Wijshoff, M. Mischi, and R. M. Aarts, "Reduction of Periodic Motion Artifacts in Photoplethysmography," *IEEE Trans. Biomed. Eng.*, vol. 64, no. 1, pp. 196–207, Jan. 2017.

[18] D. Yang, J. Zhu, and P. Zhu, "SpO₂ and heart rate measurement with wearable watch based on PPG," in *Proc. IET Int. Conf. Biomed. Image Signal Process. (ICBISP)*, 2015, pp. 2–5.

[19] P. K. Jain and A. K. Tiwari, "Heart monitoring systems—A review," *Comput. Biol. Med.*, vol. 54, pp. 1–13, Nov. 2014.

[20] G. Kolata, "Maximum heart rate theory is challenged," *New York Times*, Apr. 2001.

[21] H. S. Shin, C. Lee, and M. Lee, "Ideal filtering approach on DCT domain for biomedical signals: Index blocked DCT filtering method (IB-DCTFM)," *J. Med. Syst.*, vol. 34, no. 4, pp. 741–753, 2009.

[22] D.-G. Jang, U. Farooq, S.-H. Park, and M. Hahn, "A robust method for pulse peak determination in a digital volume pulse waveform with a wandering baseline," *IEEE Trans. Biomed. Circuits Syst.*, vol. 8, no. 5, pp. 729–737, Oct. 2014.

[23] B. A. Shenoi, *Introduction to Digital Signal Processing and Filter Design*. New York, NY, USA: Wiley, 2006.

[24] S. A. Santos, B. Venema, and S. Leonhardt, "Accelerometer-assisted PPG measurement during physical exercise using the LAVIMO sensor system," *Acta Polytech.*, vol. 52, no. 5, pp. 80–85, 2012.

[25] S. Hargittai, "Efficient and fast ECG baseline wander reduction without distortion of important clinical information," in *Proc. Comput. Cardiol.*, vol. 35. 2008, pp. 841–844.

[26] K. V. P. Naraharisetti and M. Bawa, "Comparison of different signal processing methods for reducing artifacts from photoplethysmograph signal," in *Proc. IEEE Int. Conf. Electro/Inf. Technol. (EIT)*, May 2011, pp. 1–8.

[27] M. L. Jacobson, "Auto-threshold peak detection in physiological signals," in *Proc. 23rd Annu. Int. Conf. IEEE Eng. Med. Biol. Soc.*, vol. 3. Oct. 2001, pp. 2194–2195.

[28] H. S. Shin, C. Lee, and M. Lee, "Adaptive threshold method for the peak detection of photoplethysmographic waveform," *Comput. Biol. Med.*, vol. 39, no. 12, pp. 1145–1152, 2009.

[29] B. Widrow *et al.*, "Adaptive noise cancelling: Principles and applications," *Proc. IEEE*, vol. 63, no. 12, pp. 1692–1716, Dec. 1975.

[30] W. Philips, "Adaptive noise removal from biomedical signals using warped polynomials," *IEEE Trans. Biomed. Eng.*, vol. 43, no. 5, pp. 480–492, May 1996.

[31] M. Dorbecker and S. Ernst, "Combination of two-channel spectral subtraction and adaptive Wiener post-filtering for noise reduction and dereverberation," in *Proc. Eur. Signal Process. Conf.*, vol. 1. 1996, pp. 1–4.

[32] S. Boll, "Suppression of acoustic noise in speech using spectral subtraction," *IEEE Trans. Acoust., Speech, Signal Process.*, vol. ASSP-27, no. 2, pp. 113–120, Apr. 1979.

[33] R. N. Bracewell, "The Fourier transform," *Sci. Amer.*, vol. 260, no. 6, pp. 86–95, 1989.

[34] K. G. Larkin, "Efficient nonlinear algorithm for envelope detection in white light interferometry," *J. Opt. Soc. Amer. A, Opt. Image Sci.*, vol. 13, no. 4, pp. 832–843, 1996.

[35] Q. Wang, P. Yang, and Y. Zhang, "Artifact reduction based on empirical mode decomposition (EMD) in photoplethysmography for pulse rate detection," in *Proc. IEEE Eng. Med. Biol. Soc. Conf.*, Aug./Sep. 2010, pp. 959–962.

[36] D. Sundararajan, *The Discrete Fourier Transform: Theory, Algorithms and Applications*. Singapore: World Scientific, 2001, pp. 31–94.

[37] N. Ahmed, T. Natarajan, and K. R. Rao, "Discrete cosine transform," *IEEE Trans. Comput.*, vol. C-23, no. 1, pp. 90–93, Jan. 1974.

[38] W.-H. Chen, C. H. Smith, and S. C. Fralick, "A fast computational algorithm for the discrete cosine transform," *IEEE Trans. Commun.*, vol. COM-25, no. 9, pp. 1004–1009, Sep. 1977.

[39] P. Graham. (2014). *EIMO Instant Vital Sign Monitor From iMonSys*. [Online]. Available: http://www.imonsys.com/eimo/

[40] H. H. Asada, H.-H. Jiang, and P. Gibbs, "Active noise cancellation using MEMS accelerometers for motion-tolerant wearable bio-sensors," in *Proc. IEEE Eng. Med. Biol. Soc. Conf.*, vol. 3. Sep. 2004, pp. 2157–2160.

[41] Y. Cheng, P. Jiang, and Y. Peng, "Increasing big data front end processing efficiency via locality sensitive Bloom filter for elderly healthcare," in *Proc. IEEE Symp. Comput. Intell. Big Data (CIBD)*, Dec. 2014, pp. 1–8.
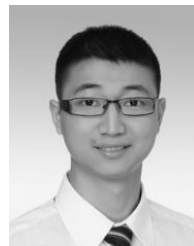
DONG YANG received the B.S. degree in automation engineering in 2014, and the M.S. degree in control engineering from Tongji University, Shanghai, China, in 2017. From 2014 to 2017, he was a Master Student with the Control Engineering Department, Tongji University. His research interests include control theory and biological/medical information.
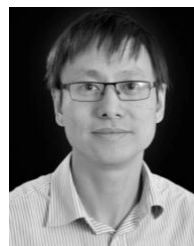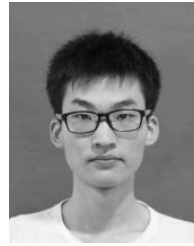
YONGQIANG CHENG is currently a Lecturer with the School of Engineering and Computer Science, University of Hull, U.K. His research interests include digital healthcare technologies, embedded systems, control theory and applications, AI, and data mining.

JIN ZHU is currently an Associate Professor with the Department of Control Science and Engineering, Tongji University, Shanghai, China. His research interests include automatic control theory and applications, robotics control, intelligent control, and industrial electronic engineering applications.

DONGFEI XUE received the master's degree in engineering from Tongji University in 2008. He is currently pursuing the Ph.D. degree with the School of Engineering and Computer Science, University of Hull. His research interests include robotics and artificial intelligence.

HANGYANG YE received the B.Eng. degree in control science and engineering from Tongji University, Shanghai, China, in 2018. He was a Visiting Student with the School of Engineering and Computer Science, Faculty of Science and Engineering, University of Hull, from 2016 to 2017. His research interests include embedded systems, wireless sensor networks, and deep learning.

GRANT ABT is a Reader in sport and exercise physiology and the Subject Group Head of Sport, Health and Exercise Science at the University of Hull. His research interests include the use of wearable devices for monitoring physical activity and exercise.

YONGHONG PENG is currently a Professor of data science and the Leader of the Data Science Research, University of Sunderland, U.K. His research interests include data science, machine learning, data mining and artificial intelligence. He is the Chair for the Big Data Task Force, and a member of Data Mining and Big Data Analytics Technical Committee of the IEEE Computational Intelligence Society. He is also a Founding Member of the Technical Committee on Big Data of the IEEE Communications and an Advisory Board Member for the IEEE Special Interest Group on Big Data for Cyber Security and Privacy. He is an Associate Editor for the IEEE Transaction on Big Data, and an Academic Editor of *PeerJ* and *PeerJ Computer Science*.

• • •